Triggering conditions and propagation of the December 2019 Palma Campania landslide: Implications for residual hazard estimation at recurrent landslide sites

Ciro Sepe [a,b], Domenico Calcaterra [a], Diego Di Martire [a], Francesco Fusco [c], Rita Tufano [a,*], Enza Vitale [a], Luigi Guerriero [a]

[a] Department of Earth, Environmental and Resource Sciences, Federico II University of Naples, Strada Vicinale Cupa Cintia 21, 80126 Naples, Italy
[b] Department of Civil and Mechanical Engineering, University of Cassino and Southern Lazio, 03043 Cassino, Italy
[c] Department of Civil and Environmental Engineering, Politecnico di Milano, Piazza Leonardo da Vinci, 32, 20133 Milan, Italy

ARTICLE INFO

ABSTRACT

Flow-like landslides triggered by rainfall are a major concern in the peri-Vesuvian region of southern Italy. On December 19th, 2019, a landslide occurred along the Crocelle slope (Sarno Mountains), which had previously experienced a similar event in February 1986. This study was conducted to assess the characteristics of this event in terms of triggering and propagation conditions and, with reference to the 1986 landslide, to evaluate the evolution of residual landslide hazards at recurring landslide sites. Data collection included field surveys, visual analysis of a Unmanned Aerial Vehicle (UAV)-based photogrammetric model, geotechnical laboratory testing, rainfall and slope stability analysis, and propagation modeling. Results suggest that the landslide i) originated below a trail, ii) involved an initial volume of 450 m^3, which did not significantly grow due to the limited entrainment of slope sediments, iii) was initiated after 13 h of rainfall (return period ~4 years), and iv) propagated along a channel with an estimated velocity of up to 10 m/s. Comparison of the 2019 event with the 1986 event revealed a significant difference in terms of landslide magnitude (i.e., volume), potentially due to the occurrence of multiple events, which may have led to the temporal depletion of available materials along a slope repeatedly affected by landslides, and possibly to the different behavior of primary layered deposits (involved in the 1986 event) compared to reworked deposits (involved in the 2019 event). This suggests a reduction in the residual landslide hazard associated with a decrease in the expected magnitude and frequency of prospective events.

1. Introduction

Rainfall-induced shallow landslides involving pyroclastic soils are a pervasive problem in many regions of the worldwide, including Java Island in Indonesia (Muntohar et al., 2022), Hong Kong in China (Chen and Lee, 2004), Mexico, El Salvador, and Honduras in Central America (Capra et al., 2003; Harp et al., 2009; Smith et al., 2015) and Italy (e.g., Del Prete et al., 1998; Calcaterra et al., 1999; Calcaterra and Santo, 2004; Fiorillo et al., 2019). In the last century, multiple rapid rainfall-induced landslides have had a harmful impact on the peri-Vesuvian and Phlegraean slopes of the Campania region in southern Italy, leading to substantial economic losses and numerous fatalities (e.g., 318, 1954 Vietri-Maiori landslides, Fiorillo et al., 2019; 160, 1998 Sarno-

Quindici landslides, Del Prete et al., 1998). Consequently, these phenomena have received considerable attention from the scientific community. In particular, numerous studies have focused on determining the critical rainfall conditions required for triggering in unsaturated soil cover (e.g., De Vita et al., 2013; Greco et al., 2013; Napolitano et al., 2015; Urciuoli et al., 2016; Damiano et al., 2017; Fusco et al., 2019, 2021; Sepe et al., 2021a, b; Tufano et al., 2021a). Further research has analyzed the predisposing contributory action of i) the geomorphologic characteristics of the affected slopes, ii) the spatial variability of stratigraphic setting, and iii) the textural properties of the involved pyroclastic covers in predisposing the slope to failure (e.g., Guadagno et al., 2005; Tufano et al., 2016; Santo et al., 2018; Greco et al., 2021). Additionally, such phenomena' post-failure mechanisms and

---

propagation characteristics were explored using empirical and deterministic models (e.g., Revellino et al., 2013; Cuomo et al., 2014). Although different terms have been employed to classify these fast-moving landslides (i.e., debris flows, debris avalanches, debris-avalanche-flows, flow-slides, mudflows, soil slips-debris flows), the scientific community generally agrees that these phenomena can be described as flow-like landslides (Iverson, 2000; Hungr et al., 2014). Typically, they initiate as shallow translational (or rotational) debris slides (Hungr et al., 2014) and subsequently evolve into debris avalanches and/or debris flows (Hungr et al., 2014). Commonly, the detachment zone is of limited extent (few m^2) and often located i) at the top of artificial cuts, ii) at the top of natural scarps or iii) in the vicinity of hollows and zero-order basins (Guadagno et al., 2005; Di Crescenzo and Santo, 2005; Cascini et al., 2008), where debris sliding is facilitated by slope geometry. Transformation into flow generally occurs after fragmentation of the sliding mass and due to sequential undrained loading and associated mass fluidization (Hungr et al., 2014). Debris avalanches typically occur along open slopes and take on a trapezoidal shape, whereas debris flows are normally funneled into pre-existing gullies and first- or second-order drainage channels. In both cases, the initial volume of the landslide may increase substantially due to the mobilization of slope material and entrainment into the moving flow (Hungr and Evans, 2004; Iverson, 2012). For instance, an initial landslide volume of several tens of cubic meters may reach several thousand of cubic meters, and this process is controlled by the amount of slope material available for mobilization. The accumulation zone is usually located at the foothill and may correspond to a pre-existing alluvial fan (Del Prete et al., 1998).

Landslide initiation is often linked to intense precipitation events and depends on prior hydrological conditions. Such conditions can modulate the hydrologic response of a slope subjected to rainfall (e.g., Rianna et al., 2014; Napolitano et al., 2016; Fusco et al., 2017) and are responsible for variations in critical rainfall characteristics required for landslide initiation. Therefore, rainfall thresholds are commonly used to identify critical precipitation and associate landslide initiation and are used as a basis for developing early warning systems (Canli et al., 2018; Conrad et al., 2021). Numerous studies have identified rainfall thresholds for landslide initiation over the peri-Vesuvian area, using both empirical and physics-based approaches. Empirical rainfall thresholds relate rainfall information to the observed landslide occurrence and are typically based on rainfall intensity and duration (Caine, 1980). Physics-based rainfall thresholds can be derived by deterministic hydrological modeling (often through variably saturated flow equations, e.g., Zhu et al., 2022) and associated slope stability analysis (e.g., Montgomery and Dietrich, 1994; Godt and McKenna, 2008; Marin et al., 2020). With respect to the Sarno Mts. area, empirical rainfall thresholds were initially proposed by Guadagno (1991). Subsequently, other authors have developed rainfall thresholds based on this approach, such as Calcaterra et al. (2000a), De Vita and Piscopo (2002), and Tufano et al. (2019), whereas physics-based rainfall thresholds were initially developed by De Vita et al. (2013). Additionally, Napolitano et al. (2016) and De Vita et al. (2018) accounted for the effect of prior hydrological conditions on rainfall thresholds by considering monitoring data.

Landslide detachment commonly occurs at slope angles ranging from 35° to 45°, while angles between 26° and 30° characterize transition zones (Calcaterra et al., 2003; Guadagno et al., 2005; Di Crescenzo and Santo, 2005). Stratigraphic reconstructions of the detachment and transit zones have demonstrated that typical successions of pyroclastic deposits are composed of variably weathered cineritic intervals, pumice levels, and paleosols (Calcaterra et al., 2000b; De Vita et al., 2013; Revellino et al., 2013; Tufano et al., 2021b). Less frequently, reworked pyroclastic deposits, in which no discernible layering is visible, have been observed in landslide detachment zones. The slip surface of the upper debris slide typically occurs within the lower part of the pyroclastic cover, resulting in much of the material being removed along the landslide path during the event propagation. This condition, typical of single-event debris avalanches (Hungr et al., 2014), is of particular
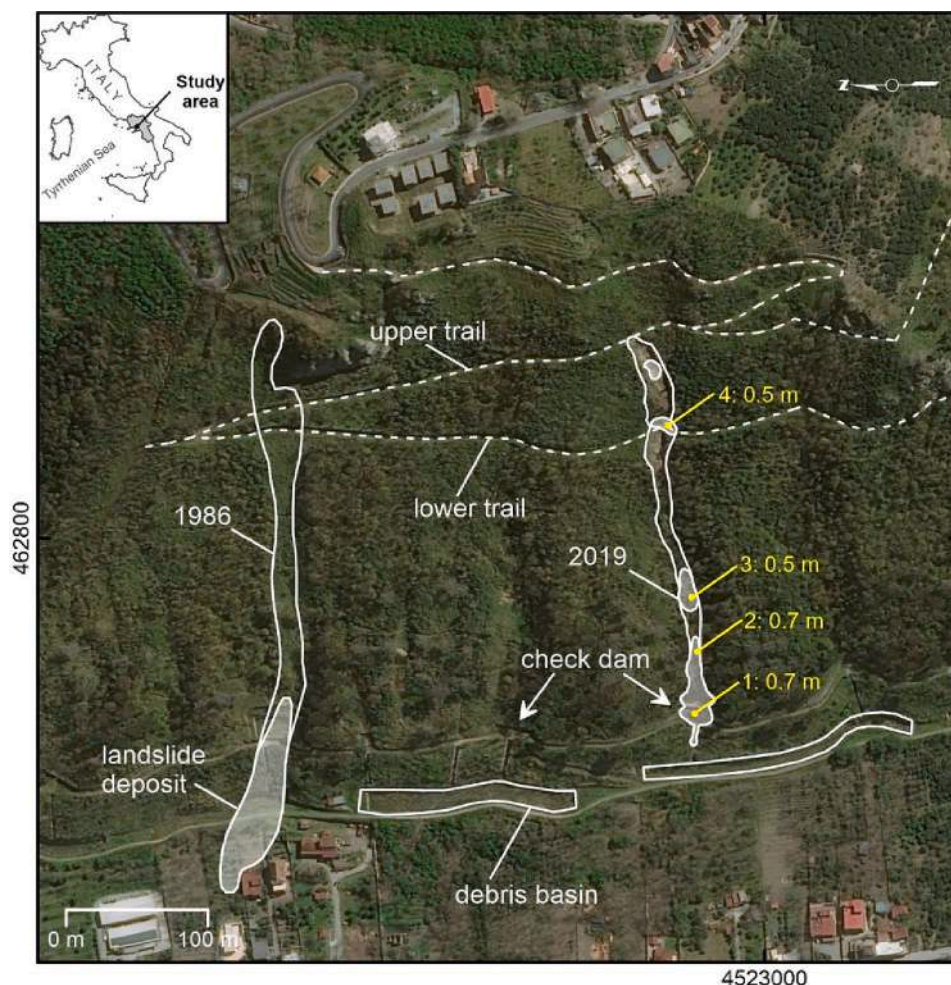
importance in terms of susceptibility and hazard assessments, as zones previously affected by fast-moving landslides (i.e., debris slide–debris-avalanche/debris flow; Hungr et al., 2014) may not be able to sustain the generation of a new event of similar magnitude due to the lack of adequate sediment supply for volumetric growth. This is significant in the context of residual hazard analysis, especially in urbanized areas (Di Martire et al., 2012; Yang et al., 2022).

On December 19th, 2019, a rapid landslide occurred at Palma Campania, on the Crocelle slope (north-western sector of the Sarno Mts.), with no casualties or damage to settlements due to the effectiveness of existing mitigation measures. The landslide was triggered by an intense rainfall event with a total height of approximately 99 mm and a duration of approximately 20 h, peaking at 22 mm/h. Therefore, its propagation was mainly confined to a slope channel that directed the flow toward the slope base. This landslide was only the most recent in a series of events to affect the Crocelle slope, the most severe being an incident in February 1986 that caused eight fatalities and damaged settlements (Guadagno et al., 1988). Consequently, in 2008, mitigation measures were installed at the footslope, including check dams at the slope channel section at the base of the slope and retention basins at channel outlets.

On this basis, an analysis of the characteristics of the event in terms of initiation and propagation is presented here to discuss local implications for residual hazard estimation and evolution. Specifically, results from i) Unmanned Aerial Vehicle (UAV)-aided field survey, ii) geotechnical laboratory testing of slope materials, iii) rainfall and related slope stability analysis, and iv) propagation modeling are interpreted in the context of residual hazard estimation at locations already impacted by fast-moving landslides. In this perspective, the landslide that occurred in 1986, involving primary layered pyroclastic deposits, is considered a reference scenario, and the new event, involving reworked materials, is viewed as a possible subsequent event. Although the events occurred at separate sites, initiation conditions (i.e., sedimentologic characteristics of involved deposits) suggest that the events occurred in two distinct and successive evolutionary steps of slope evolution likely subsequent landslides. This work, providing an innovative model of landslide residual hazard evolution for slopes covered by pyroclastic deposits, is a considerable novelty in the context of hazard analysis. However, to the authors' knowledge, no specific contributions in this sense have been provided. Furthermore, the significance of this paper is increased by the newly provided perspective in assessing residual hazard that would decrease over time as a function of the potential landslide magnitude. As a result, current approaches to residual hazard assessment, based on magnitude-equivalent scenarios, could lead to hazard overestimation. In addition, the recent Palma Campania landslide interacted with existing mitigation measures, providing an opportunity to evaluate their mitigating effect in relation to the event's magnitude.

2. Study area

The Palma Campania landslide is located at approximately 462,933 E and 4,523,086 N (UTM 33 coordinates; Fig. 1) and involves pyroclastic deposits covering the so-called Crocelle slope, part of the western slope of Mt. Sant'Angelo, within the Palma Campania Municipality (eastern border of the Campanian plain). In terms of the primary geological-stratigraphic context, the study region is characterized by the presence of Mesozoic carbonates (Patacca and Scandone, 2007) that are overlayed by soils of pyroclastic origin (Upper Pleistocene–Holocene), which are attributed to the volcanic activity of the Somma-Vesuvius volcano and, in a lesser extent, the Phlegraean Fields (the western portion of the Campania plain; De Vita et al., 2013). Furthermore, anthropogenic deposits comprising reworked materials due to road cutting and debris deposits, occasionally mixed with pyroclastic materials, are present. The Mesozoic complex consists primarily of Cretaceous limestones belonging to the stratigraphic-structural unit of Picentini-Taburno Mts. (Vitale and

Fig. 1. Map showing the position and extent of both 1986 (from Guadagno et al., 1988) and 2019 Palma Campania landslides. Main trail and mitigation measures consisting of check dams and debris basins are shown. Yellow dots indicate landslide deposit thickness. UTM 33 N coordinates are shown at the map edges. (For interpretation of the references to colour in this figure legend, the reader is referred to the web version of this article.)

Ciarcia, 2018), which is well-exposed along the western side of Sant'Angelo Mt. (762 m a.s.l.). This carbonate structure is usually fractured and karstified, predominantly in the upper part. The thickness of the overlying pyroclastic and/or detrital deposits ranges from 0.5 up to 2.0 m. The stratigraphic composition of the covering soils is characterized by alternating Vesuvian eruptions of "Ottaviano" (8900 BP) and "Avellino" (4365 BP) (Santacroce et al., 2008) deposits and pedogenized horizons. The Crocelle slope is characterized by angles between 35° and 45° and parallel slope incisions due to intense morpho-evolutionary processes.

On February 22nd, 1986, the Crocelle slope and its covering pyroclastic deposits were subject to a rapid landslide, as documented by Guadagno et al., (1988; Fig. 1). The source region of this landslide, in comparison to that occurred in 2019, was situated ca. 250 m northward and at an approximate altitude of 250 m above sea level, involving an approximate volume of 15,000 m^3 of material and propagating down-slope for roughly 40 m along a channel. This event resulted in the destruction of two buildings at the base of the slope, as well as the loss of eight lives. The landslide deposit extended beyond the foot of the incline for approximately 40 m, with an angle of repose of approximately 28°. This event occurred in the aftermath of a rainy period extending from January 31st to February 26th and saw a total of 290 mm of rainfall.

3. Methods

3.1. UAV photogrammetry-aided field surveys

A field survey was conducted at the beginning of 2020 to decipher landslide characteristics, such as the lithology of involved materials, and the position of the source zone relative to potential predisposing conditions (e.g., road cuts, rocky scarps, etc.), geometry and stratigraphic settings of the source zone, including source material thickness, the geometry of the propagation path along the involved channel, basal erosion distribution in the transit zone, thickness of landslide deposit, presence of involved woody debris, and distribution of landslide deposit in relation to existing mitigation measures. Visual inspection of exposed material was employed to identify the lithologic and sedimentologic features of the involved material, including top-soil horizons. Manual field measurements were taken at selected locations to estimate the source and transit zone width, source material and deposit thickness, and erosion depth along the path. Smartphone-aided field mapping was used to construct a digital model of the landslide deposit. Due to the inaccessibility of certain slope sectors for landslide geometry reconstruction, an UAV photographic and photogrammetric survey was performed to generate a slope model suitable for landslide geometry measurements, path reconstruction, and source volume estimation. The survey was conducted with an overlap of around 80% and a side lap of approximately 60%. Additionally, the Real Time Kinematics Global Positioning System Technique (RTK GPS) was used to acquire six control

points with a 3D accuracy of 2 cm to ensure image alignment and elevation. The acquired images were then processed to generate a post-event Digital Surface Model (DSM) and Digital Elevation Model (DEM) with a 1-m single-sided pixel dimension, which was used to estimate the landslide source volume by differencing and volume computation.

3.2. Laboratory testing

To support both landslide stability and propagation analysis, understanding the physical and mechanical properties of the involved soils, laboratory tests were conducted on samples taken near the source zone and along the upper sector of the transit zone. Samples were acquired by pushing a hand-driven steel sampler into the material after the construction of shallow pits. Medium and low-grade disturbed samples were obtained to estimate the water content, specific gravity, unit weights, and grain size distribution (ASTM Standards, D 2216, D 854, D 2937, D 422, respectively; ASTM 2008). For mechanical soil characterization in pre-landslide conditions, direct shear tests were performed on reworked samples at increasing stress levels, namely 100, 200, and 300 kPa. Direct shear tests were executed with a standard displacement-controlled apparatus according to ASTM D 3080–90. The displacement rate was established at 0.120 mm/min. Micrometer dial gauges with a 0.001 and 0.01 mm resolution were used to measure vertical and horizontal displacements, respectively. Shear strength and corresponding Mohr–Coulomb mechanical parameters (c', φ') were estimated.

3.3. Rainfall analysis

An analysis of boundary conditions for landslide initiation was conducted through a statistical analysis of the maximal rainfall triggering the 2019 landslide for various durations. Rainfall data were acquired from the Palma Campania rain gage (ID 37261) via the "Centro

Funzionale Multirischi della Protezione Civile Regione Campania" (http://centrofunzionale.regione.campania.it/) an entity of the public sector which is dedicated to meteorological forecasting, monitoring and assessing current and/or anticipated hydraulic and geological issues as support to the Civil Protection Department. Rainfall data registered from 2008 to 2021 as 10-min time series were eventually accumulated for certain durations, namely 1 h, 3 h, 6 h, 8 h, 12 h, and 24 h, and the annual maxima for each duration was estimated (Fig. 2).

Subsequently, a statistical analysis was conducted using the Gumbel frequency distribution model (Generalized Extreme Value Type I; Jenkinson, 1955) in the form of a Cumulative Distribution Function (CDF). This model expresses the probability function P(h) as:

$$P(h) = exp\{-exp[-\alpha(x-u)]\} \tag{1}$$

where the parameters α and u are estimated considering the mean value of the series (μ) and its standard deviation (σ) as follows:

$$\alpha = \frac{1.283}{\sigma} \tag{2}$$

$$u = \mu - 0.45\,\sigma \tag{3}$$

The inverse of the CDF (i.e., a survival distribution function) provides the values of the cumulative rainfall for a specific duration, allowing for the determination of the return period (T) for the assigned rainfall intensity and related duration at each point of the function. The rainfall triggering the December 2019 landslide (Fig. 3) was also evaluated by estimating the return period of the maximum values for the specific durations using the estimated Gumbel distribution parameters.

3.4. Hydrological modeling and slope stability analysis

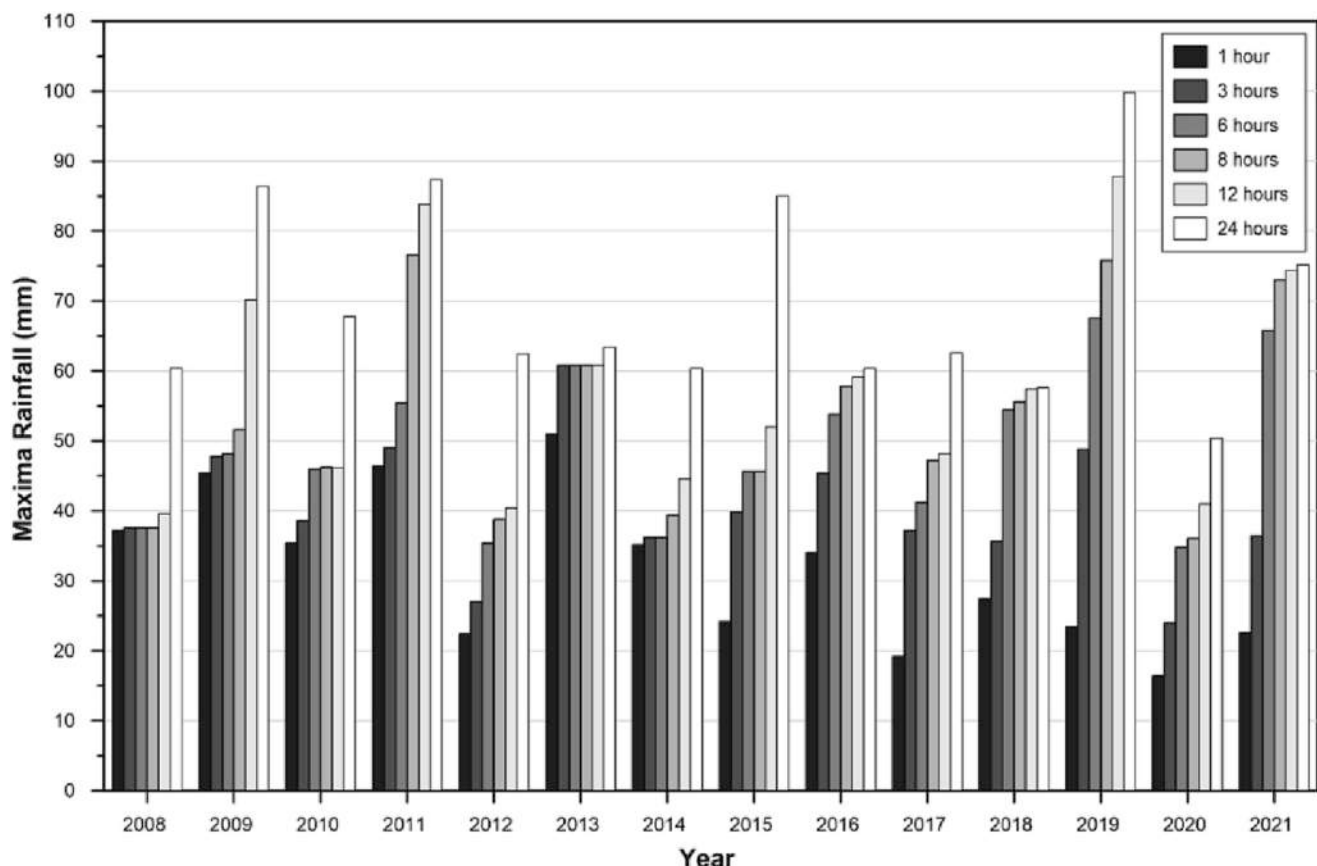The numerical code VS2D (Hsieh et al., 2000) was utilized to

Fig. 2. Rainfall annual maxima from 2008 to 2021 for 1 h, 3 h, 6 h, 8 h 12 h, and 24 h. Data were derived from the Palma Campania rain gage.
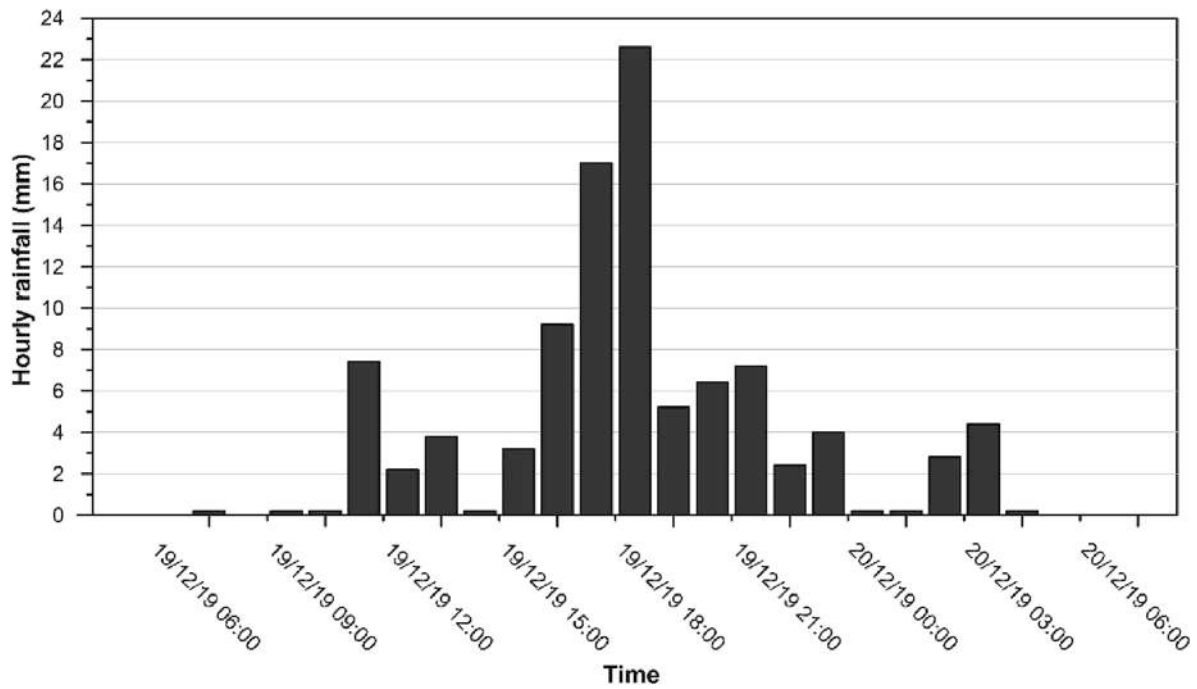
Fig. 3. Hourly rainfall depicting the characteristics of the storm responsible for 2019 landslide initiation.

evaluate the hydrological response modeling and stability of a hillslope. This code is based on Richard's equations and simulates two-dimensional variably saturated subsurface flow by solving the flow equation. The model combines the law of conservation of fluid mass with a non-linear form of Darcy's equation using the finite-difference method. However, due to lacking a general analytic solution, numerical approximations of spatial and temporal derivatives are necessary. Prior studies have used the VS2D model to simulate the hydrological behavior of pyroclastic soils in various test areas within the Campania region, comparing modeled results with field monitoring of the pressure head (Napolitano et al., 2016; Fusco et al., 2019).

The numerical model was established based on a pre-landslide axial longitudinal cross-section of the slope, which started upslope from the road cut above the landslide, according to both field observations and the reconstructed engineering-geological model. This profile was constructed by comparing the obtained photogrammetric DEM with the available pre-landslide LiDAR-derived DEM.

The physical and mechanical characteristics of the affected slope materials were determined by laboratory testing. Furthermore, hydro-mechanical properties of the carbonate bedrock and anthropogenic deposits (constituting the road) were assigned based on previous studies (De Vita et al., 2013; Table 1). Additionally, unsaturated and saturated hydraulic soil properties were assigned using fitting parameters of the van Genuchten (1980) SWRC model and assigned hydrological

Table 1
Saturated (K_{sat}) and unsaturated parameters for van Genuchten's formula for the SWRC, derived from bibliographic data (De Vita et al., 2013) and the VS2D library. Key to symbols: K_{sat}—hydraulic conductivity, Ss - specific water storage, RMC—residual volumetric water content, and α and β - van Genuchten (1980) model fitting parameters.

Lithology	K_{sat} (m/s)	S_S	n	RMC	α	β
Present-day soil	4.28×10^{-5}	0.0500	0.500	0.08	5.60	1.57
Anthropogenic deposits	4.63×10^{-3}	0.0004	0.375	0.02	4.31	3.10
Carbonate bedrock	1.37×10^{-7}	0.1400	0.200	0.02	4.31	3.10

properties.

Boundary conditions for hydrological modeling incorporated a vertical flux across the ground surface, to which the inciting rainfall event (Fig. 3) was assigned. Specifically, the rainfall event, totaling 99.2 mm, lasted approximately 20 h with an average intensity of 4.88 mm/h. Additionally, the effect of water loss due to the evapotranspiration process was considered negligible due to the dormant period that characterizes the vegetation (i.e., winter season). The downstream and basal boundaries of the model domain were set as seepage faces, accounting for the absence of an impermeable horizon. The upstream boundary was configured as a no-flow boundary. The initial pressure head (PH) used for the simulations was established according to the typical winter conditions of the ash-fall pyroclastic cover observed in the Sarno Mts. area (i.e., Fusco and De Vita, 2015; Fusco et al., 2017). Finally, based on results from hydrological modeling, a limit equilibrium slope stability analysis was performed. Driving forces were computed along the reconstructed failure surface, which was assumed to correspond to the presently exposed surface due to the minimal effect of erosional phenomena. Resisting forces were estimated according to a suction stress model (Lu and Likos, 2004) for which the suction stress, σ^s, is considered equivalent to the pore water pressure in saturated conditions while corresponding to the product of the degree of effective saturation and matric suction for partially saturated conditions.

$$\sigma^s = -(u_a - u_w) \, for \, (u_a - u_w) \leq 0 \qquad (4)$$

$$\sigma^s = -\theta_e(u_a - u_w) \, for \, (u_a - u_w) \rangle 0 \qquad (5)$$

where u_a is the pore air pressure and u_w is the pore water pressure.

The Factor of Safety (FoS) can be determined using the equation for infinite slope stability (e.g., Chang et al., 2021; Sun et al., 2021):

$$FoS = \frac{c' + [\sigma \cos^2\beta - \sigma^s]tan\varphi'}{\sigma \sin\beta \cos\beta} \qquad (6)$$

where c' is the effective cohesion, σ is the total stress, φ' is the friction angle, and β is the slope angle. For the computation of the FoS, pressure head, and water content values were considered for each simulation time step along five vertical profiles, with either five (V1, V2, V3) or six (V4, V5) observation points spaced 0.50 m apart in depth.

These data allowed for estimating the FoS for each point of each vertical profile, accounting for the variation in pressure head resulting from rainfall. The FoS was calculated for each time step (600 s) of the numerical simulation to assess the critical duration of the rainfall event that could lead to slope instability (FoS = 1).

3.5. Propagation modeling

Propagation modeling of the landslide was conducted employing the Smoothed Particles Hydrodynamics method (Benz, 1990; Monaghan, 1992) as implemented in the DAN-3D software (McDougall and Hungr, 2004). DAN-3D is based on a numerical solution of the depth-averaged Lagrangian equations of motion for an "equivalent fluid" (Hungr, 1995), thus allowing for simulating the propagating landslide mass as a hypothetical material governed by a simple rheological relationship. The model can describe the motion of the mass in terms of its dynamic characteristics, including total runout distance, velocity and discharge of the flowing mass, and thickness distribution (both instantaneous and maximum). As a quasi-3D model, DAN-3D does not require a pre-defined landslide path but rather computes it based on the available post-event DEM of the slope. The necessary inputs for such a simulation include: i) a post-event DEM of the affected slope, ii) a reconstructed thickness distribution of the source volume, and iii) physical, mechanical, and rheological parameters of the landslide material (unit weight, dynamic friction angle, etc.). Furthermore, material entrainment during flow propagation can be modeled, providing a mapped distribution of slope materials and their characteristics, an erosion rate, and the maximum thickness of erodable material. The erosion rate and the rheological model employed, along with its associated parameters, need to be calibrated based on field observations (e.g., landslide path geometry including final elongation, deposit distribution, and local thickness,

estimated velocity, etc.; e.g., Revellino et al., 2004, 2013).

In the case of the recent Palma Campania landslide, the Voellmy (1955) rheological model, modified by Hungr (1995), was chosen for propagation modeling. This model considers the resistance to motion at the base of the propagating flow to be expressed as:

$$\tau = \gamma H \left(cos\alpha + \frac{\alpha_c}{g} \right) f + \gamma \frac{v^2}{\xi} \tag{7}$$

where τ denotes the resisting stress at the base of the flow, γ denotes the unit weight of the flowing material, H denotes the flow depth, α denotes the slope angle, f denotes the dynamic friction coefficient related to the total normal stress at the base of the flow, α_c denotes the centrifugal acceleration resulting from the vertical curvature of the flow path, and ξ denotes a turbulence coefficient, m/s^2. Material properties, such as unit weight, were derived by laboratory testing, while the dynamic friction coefficient and turbulence coefficient were estimated using trial and error, considering the extent of landslide and deposit thickness measured at the selected locations. Best results were obtained for an f of 0.2 and a ξ of 200 m/s^2. The parameterization was consistent with previous studies of analogous events (e.g. Revellino et al., 2013). Since the field survey revealed only minimal (<0.1 m) and localized erosion along the landslide trajectory, material entrainment was not considered in this propagation analysis. The analysis output comprised a temporal map of flow depths, a map of post-event sediment distribution, and a map of maximum velocities.

4. Results

4.1. Landslide characteristics and material properties

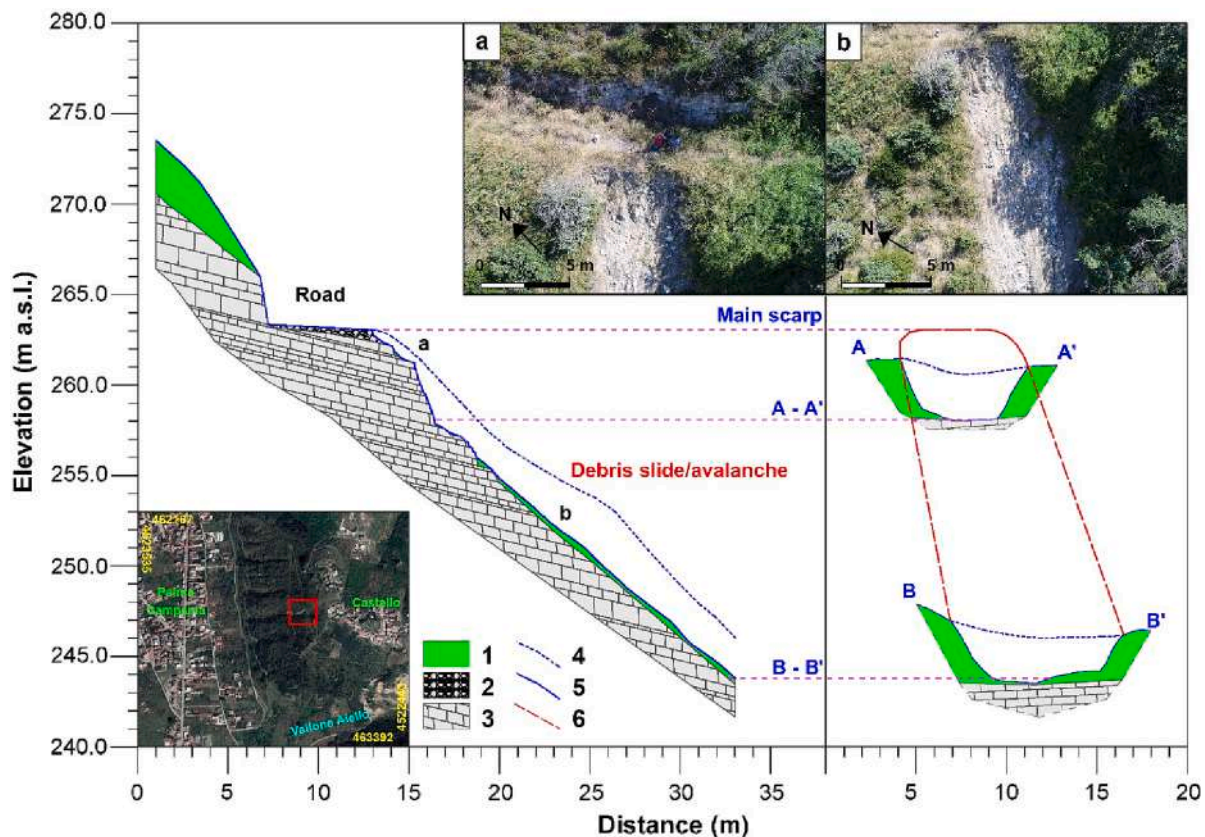Figs. 1 and 4 present the results of the observations and

Fig. 4. The geological model of the detachment zone reconstructed using data from field investigations: (1) present-day top-soil (A and B soil horizons), (2) anthropogenic deposits, (3) carbonate bedrock, (4) pre-landslide slope profile, (5) present-day slope profile, and (6) geometry of the landslide detachment zone. Inset pictures show the detachment zone and the associated trail.

measurements carried out in the field and through the analysis of the available LiDAR DEM and the DSM derived from the photogrammetric analysis of UAV-based images. It is evident that the Palma Campania landslide in December 2019 has an axial length of approximately 300 m, a width of the source zone of ~10 m, and a maximum width of the deposit of ~25 m. The detachment zone has a generally rectangular planar form and a concave longitudinal cross-sectional shape; it covers an area of roughly 400 m². As illustrated by the longitudinal and cross sections in Fig. 4, the average thickness of the affected pyroclastic material is ~1.2 m, with an initially estimated volume of the landslide, derived from DEM differencing, of ~450 m³.

The landslide was initiated at 260 m above sea level, below a trail traversing the slope. The material involved in the initial slide was characterized by brown reworked pyroclastic material, whose primary stratification, typically associated with such deposits in the region, had been eroded. This material appears to be composed of a combination of weathered ashes, pumice, and slags, with some calcareous clasts. The slope was predominantly covered with shrubs and a few individual trees. During the field inspection, it was observed that the landslide had removed most of the pyroclastic cover, exposing the underlying carbonate bedrock. Additionally, sample sediment entrainment due to the sliding was observed along the upper sector of the transit zone, with an average erosion depth of ~0.1 m. Moreover, dispersed deposits of reworked pyroclastic material were observed along the lower edge of the detachment zone and transit zone, with a maximum thickness of <1 m. The slope angle along the landslide path varied between 41° in the detachment zone, 40° in the transit zone, and 20° in the deposition zone. The landslide deposit at the base of the slope was fan-shaped, with a maximum thickness of ~1 m and containing woody debris. This indicates that the landslide may have initiated as a debris slide before propagating along a slope-parallel channel as a debris flow.

Laboratory testing on medium and low-grade disturbed samples of pyroclastic material involved in the landslide revealed that the soil consists of slightly gravelly sand with silt. The average water content at the time of sampling was 23%. Specific gravity was calculated to be 2.38 g/cm³, with a corresponding unit weight of ~11 kN/m³, and an estimated porosity of 64%. The grain size distribution indicated a D_{60} of 0.347 mm and a D_{10} of 0.009 mm, yielding a uniformity coefficient of 38.5. Results of direct shear tests in terms of stress-strain curves and related Mohr–Coulomb failure envelope are presented in Fig. 5.

Samples tested at stress levels of 100, 200, and 300 kPa demonstrate ductile and contractile behavior. As illustrated in Fig. 5c, the samples demonstrate a progressive increase in stiffness and shear strength with escalating normal effective stress. The Mohr–Coulomb failure envelope corresponding to the end-of-test shear strengths is displayed in Fig. 5e. The interpretation of the results in terms of shear strength parameters suggests a friction angle of approximately 43° and a zero cohesion value.

4.2. Conditions for landslide initiation

Fig. 3 illustrates the characteristics of the duration and distributed intensity of the rainfall events responsible for initiating the 2019 landslide. The probabilistic analysis of the annual maxima of the rainfall time series enabled the estimation of the Gumbel distribution frequency parameters and the derivation of the return period of the maxima of the rainfall, which triggered the 2019 landslide for the considered durations. Fig. 6 depicts the curves of return periods for the annual maxima rainfall series for cumulative rainfall and specified duration. Also shown is the path corresponding to the return period of the maximum values of the cumulative rainfall, which triggered the 2019 landslide. The results indicate that for durations of 1 and 3 h, the triggering rainfall has a return period ranging from 1 to 3.5 years. For 6 h, the return period reaches values close to 10 years. For 8-h' duration, the return period decreases to 5.5 years, subsequently exceeds 10 years for a duration of 12 h, and reaches 12.5 years for a duration of 24 h.

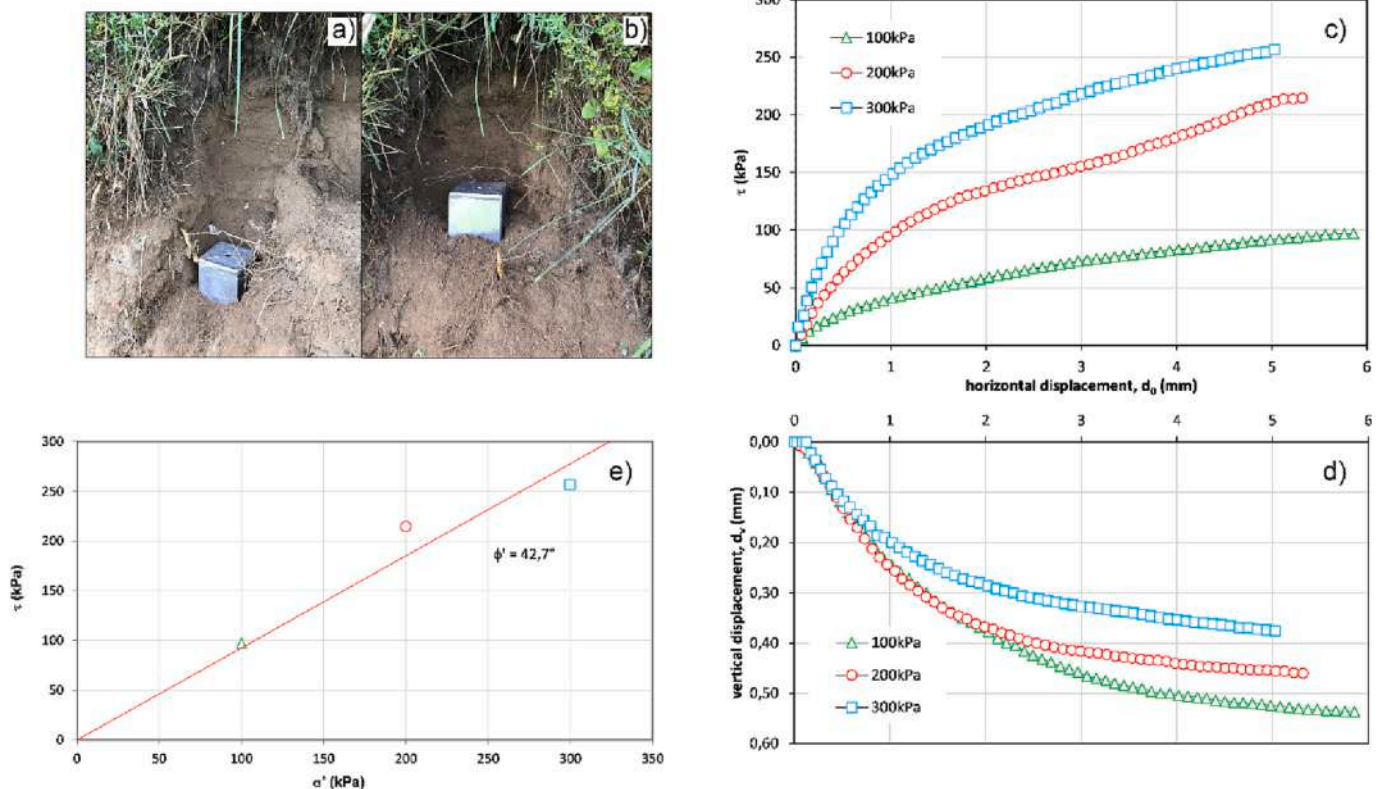The reconstructed two-dimensional numerical model was

Fig. 5. In situ soil sampling phase - a), b) and direct shear test results: stress-strain curves of samples at increasing stress levels (i.e., 100, 200 and 300 kPa) - c) τ, d_o - d) d_v, d_o - e) end-of-test failure envelope.
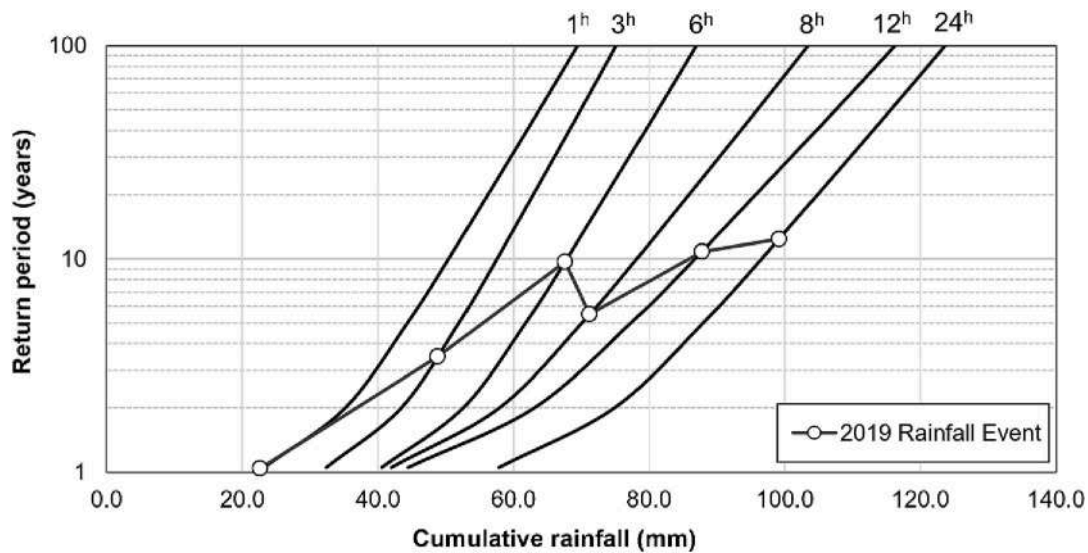
Fig. 6. The return period for cumulative rainfall related to specific durations of 1 h, 3 h, 6 h, 8 h, 12 h, and 24 h was derived from the statistical analysis of the maxima rainfall data. Return periods of maxima rainfall of the event triggering the 2019 landslide are also shown.

representative of the source zone (Fig. 7) enabled numerical simulation of the slope hydrological response to modeled rainfall events in terms of PH distribution. During the simulated rainfall (Fig. 3), a gradual increase in PH and a decrease in FoS values were observed in the lower part of the pyroclastic deposits covering the slope and downslope of the artificial cut (Fig. 8A). The effect of the increase in PH strongly influenced V1 and V2 vertical profiles, where saturated/near saturated conditions were simulated, leading to instabilities. Specifically, an unstable condition (i. e., FoS < 1) was estimated at a depth of 2.00 m along the V1 vertical profiles (Fig.s 8A-a and 8B) after ~13 h (45,600 s) of rainfall and an approximate total rainfall height of about 73.2 mm. Additionally, FoS > 1 characterized V2, V3, V4, and V5 vertical profiles, although a rise in PH was observed (Fig. 8C).

4.3. Landslide propagation

Fig. 9 (a to d) presents the results of the landslide propagation modeling along the Crocelle slope from the detachment zone to the slope base depicting flow thickness and the area affected. Specifically, 10 s after the detachment (Fig. 9a), the landslide mass (i.e., the flow front) had advanced ~45-m downslope, entering the parallel slope creek and reaching the lower segment of the trail, downslope from the detachment zone. In the initial propagation stage, the landslide mass assumed a fan-like shape, likely reflecting the transition from the initial slide mechanism to the subsequent flow; flow thickness reached ~1 m at the center of the mass. Twenty seconds after the detachment (Fig. 9b), the landslide mass had mostly passed through the lower trail (~95-m downslope of the detachment zone), and only a small remnant was still traveling along the upper sector of the path above the lower trail. At this propagation stage, the front of the mass exhibited an elongated shape, constrained by the flank of the creek, characteristic of flow-like landslides. The thickness of the flow locally reached ~1 m. Forty seconds after the detachment (Fig. 9c), the front of the flow was nearing the slope base (~180-m downslope from the detachment zone), with the whole landslide mass having assumed an elongated form, moving along the slope-parallel creek. The exception was a small tail of the flow traversing the lower trail and a small suspended deposit. Sixty seconds after the detachment, the front of the flow reached the check dam at the base of the slope (Fig. 9d; ~240-m downslope from the detachment zone). The landslide mass was completely traveling along the parallel slope creek, and the thickness of the flow reached ~1 m in several locations. Two suspended deposits were identified at this propagation stage: one at the bottom edge of the detachment zone and the second at the lower trail.

Fig. 10 (a and b) illustrates the final deposit distribution along the slope and spatial velocity distribution during landslide propagation. As depicted in map a), numerical modeling suggests that after propagation, the landslide mass assumed a fan-shaped form at the slope base, producing a deposit with a maximum thickness of ~0.85 m. The landslide mass passed through the check dam, splitting the deposit into two fans: an upslope-constrained fan and an unconstrained downslope fan. The model also predicted a tail deposit, as well as two suspended deposits located in the upper sector of the slope.

The local thicknesses estimated from field measurements at points 1, 2, 3, and 4 are 0.7 m, 0.7 m, 0.5 m, and 0.5 m, respectively, which are well-correlated with local model estimates of 0.8 m, 0.76 m, 0.65 m, and 0.6 m. Additionally, the modeled area affected by the landslide
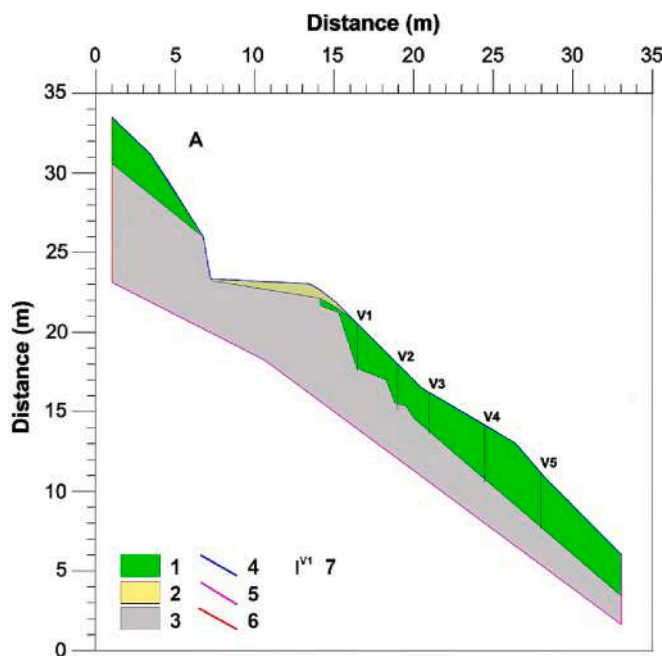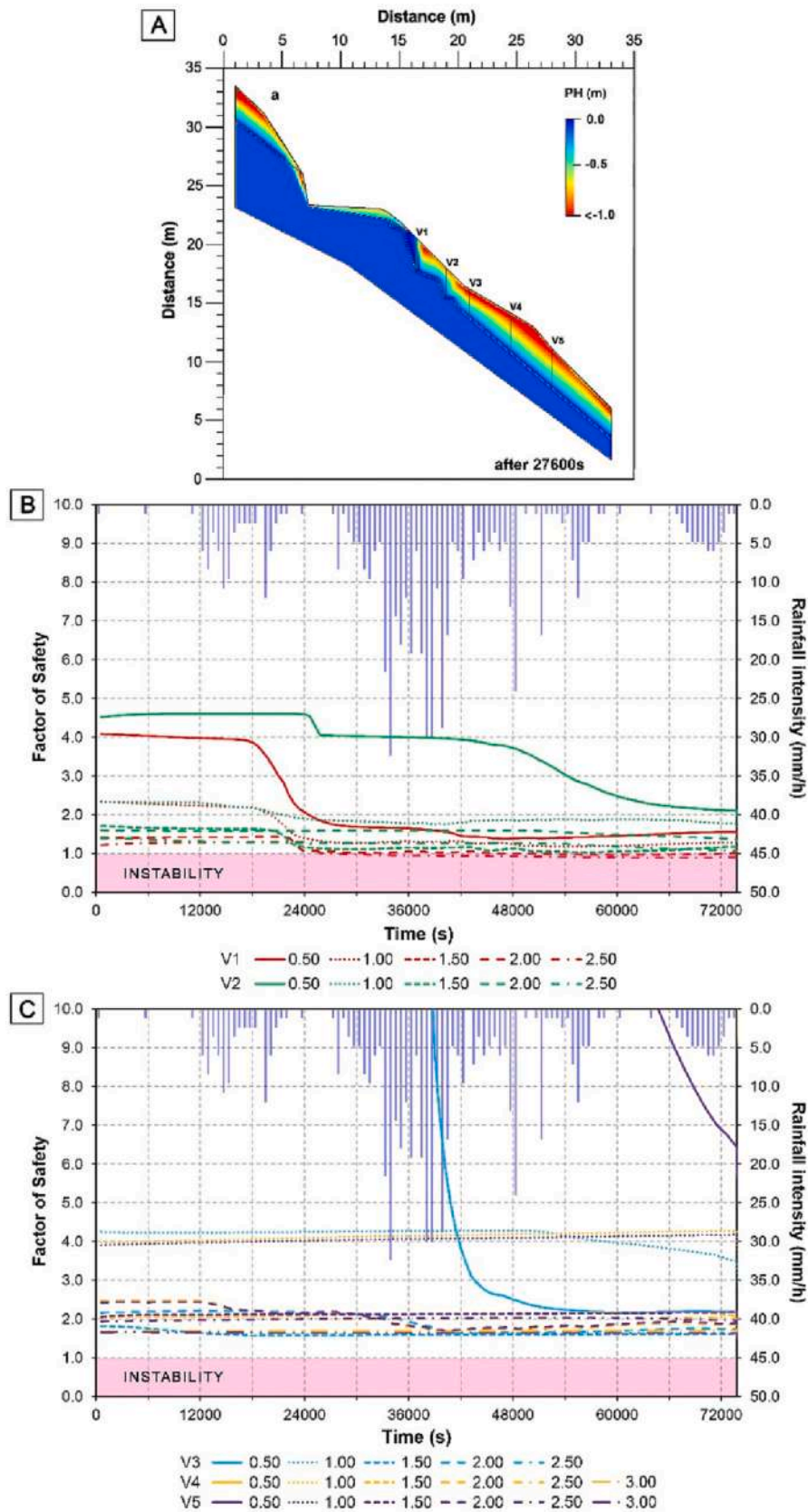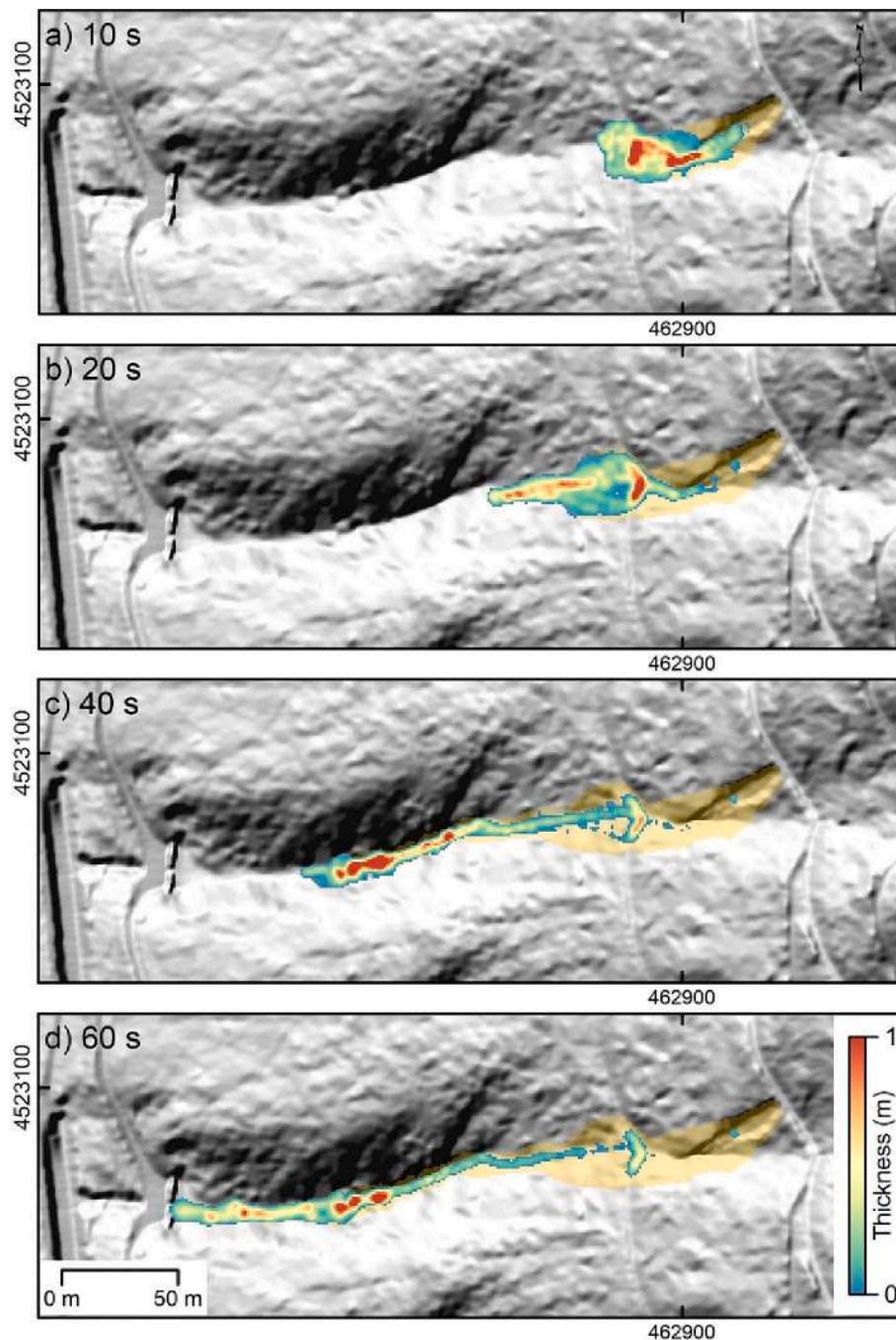

Fig. 7. The setup of the numerical hydrological model in VS2D (Hsieh et al., 2000): (1) present-day top-soil (A and B soil horizons), (2) pumiceous soil horizon, (3) carbonate bedrock, (4) rainfall boundary, (5) possible seepage face, (6) no-flow boundary, and (7) vertical profiles.

Fig. 8. Slope models showing the hydrological response obtained through VS2D modeling after 45,600 s (A). Estimated FoS variation across the vertical profiles, coinciding with specific rainfall intensities characterizing the December 19th, 2019 event, is also shown (B, C). Hourly rainfall intensity is referred to as the 10-min series.

Fig. 9. Maps showing results from propagation modeling of the December 2019 Palma Campania landslide in terms of flow thickness and involved area (orange shadow) at a) 10 s, b) 20 s, c) 40 s, and d) 60 s after the detachment. UTM 33 N coordinates are shown at the map edges.

propagation has a shape that agrees with that reconstructed from field observation (i.e., dashed line in Fig. 10a), albeit larger at the detachment where a sliding-dominating movement mechanism is expected. Map b) illustrates the landslide velocity distribution along the propagation path. As indicated by the map, the landslide accelerated up to approximately 10 m/s after the detachment, followed by deceleration as the landslide mass passed through the lower trail. Downslope, new acceleration occurred, leading to the landslide reaching a maximum velocity of ~10 m/s and subsequently decelerating at the slope base.

5. Discussion

5.1. Triggering conditions and propagation

The hydrological modeling and slope stability analysis of the 2019 Palma Campania landslide revealed that the landslide was initiated after ~13 h from the beginning of the triggering rainfall event. Based on the probabilistic analysis of the rainfall time series, the modeled rainfall event was characterized by an estimated return period of ~4 years. This value differs from the return period of the maximum hourly intensity of the triggering event (i.e., 5.5 years; Fig. 6). Consequently, the slope failure was likely due to the combined effects of antecedent hydrological conditions. The analyzed landslide occurred during the winter season
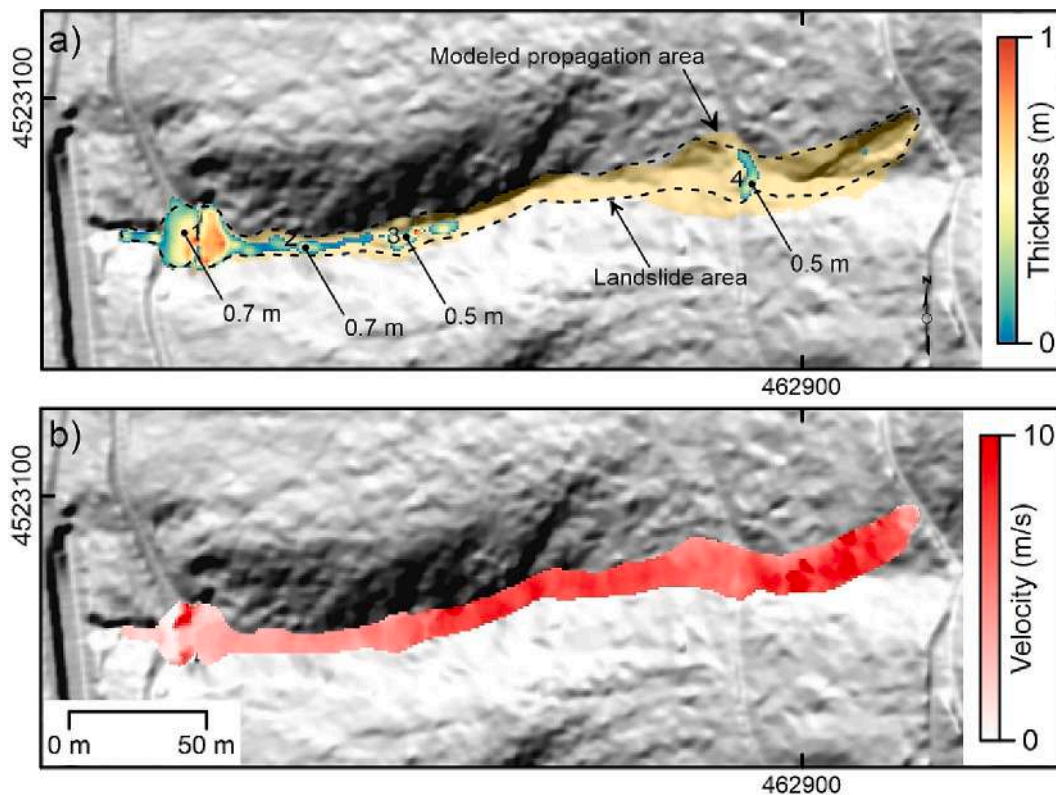
Fig. 10. Maps showing the final deposit distribution in terms of thickness (a) and velocity (b) after the propagation of the December 2019 Palma Campania landslide along the Crocelle slope. UTM 33-N coordinates are shown at the map edges.

when the significant water content of the soil cover can be attributed to both the precipitation and the dormant vegetation (Napolitano et al., 2016; Fusco et al., 2017). This can promote landslides with initiation by rainfall events of limited intensity (i.e., low return period) and long duration (Greco et al., 2013). This is supported by the observation where the rainfall intensity responsible for the Palma Campania landslide did not exceed 7 mm/h (Fig. 11).

Fig. 11 shows the rainfall conditions responsible for the modeled slope instability (i.e., the red rectangle) and the intensity-duration evolution of the triggering rainfall event. As can be seen, the instability condition occurs after a sequential increase in intensity, depicted by sub-vertical segments of the intensity-duration path. The landslide was initiated when the rainfall intensity-duration conditions approximated the thresholds proposed by Calcaterra et al. (2000a) and Tufano et al. (2019), corresponding to a return period of $1 < T < 2$ years and exceeding them.

Although the antecedent conditions for landslide initiation were set according to the monitored winter conditions for the area, the modeled landslide was consistently below the rainfall threshold developed by Napolitano et al. (2016) for the winter season. This might be due to differences between measured (and modeled) rainfall and the event that effectively triggered the slope. It is likely that the real amount of the triggering rainfall event was not recorded by the single representative rain gage as it was located at 80-m a.s.l. and about 1.8 km away from the source zone.

Furthermore, a morphological discontinuity (i.e., road cut) was located upslope of the source zone of the 2019 Palma Campania landslide. Slope geometry and local changes in slope morphology have been recognized as significant predisposing factors for landslide initiation, causing concentrated infiltration into surface flow during rainfall events and changes in the underground water circulation, as demonstrated by Di Crescenzo and Santo (2005), Guadagno et al. (2005), and Cascini et al. (2008). This effect has also been observed in different contexts,

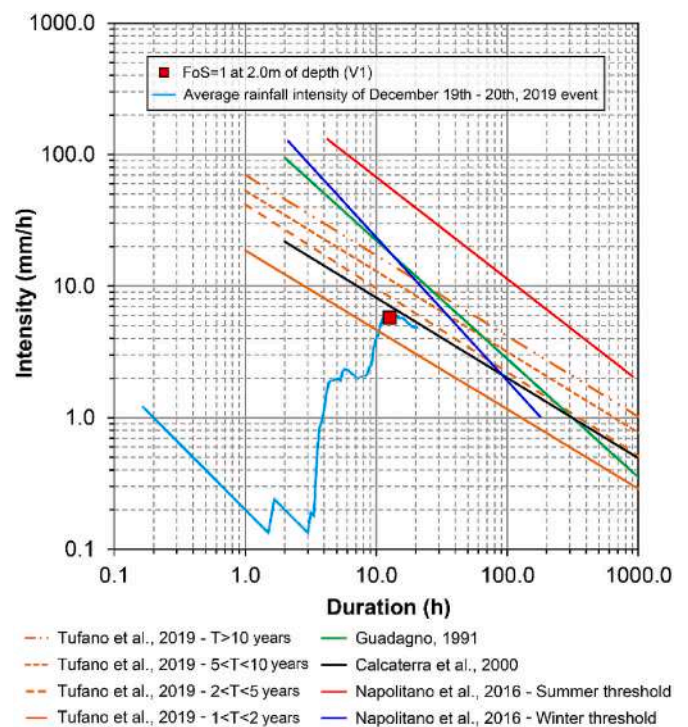

Fig. 11. Comparison between bibliographic I–D thresholds, available for Sarno Mts. area, and I–D value coinciding with the slope instability observed through VS2D modeling. The triggering rainfall event of December 19th, 2019, is also shown.

such as Asia, where the proliferation of informal local roads in the past decade has increased the risk of rainfall-induced landslides (e.g., Pradhan et al., 2022). Road cuts interrupt the morpho-stratigraphic continuity of the slope, promoting rainfall infiltration into the unsaturated zone and consequently increasing the soil water content, reducing the soil suction and shear strength (Fredlund et al., 1978; Wu et al., 2017; Rahardjo et al., 2019), leading to potential instability.

The mechanical and physical parameters determined by laboratory testing and used for the physics-based model settings showed a good correspondence with literature data estimated by Crosta and Dal Negro (2003), Bilotta et al. (2005), Cascini et al. (2005) and De Vita et al. (2013), and Tufano et al. (2021b) for peri-Vesuvian ash-fall pyroclastic soils (Table 2). The friction angle (φ') of materials forming the B horizon presented higher values than those estimated by Bilotta et al. (2005) and Cascini et al. (2005) for both the "A" and "B" classes and the B_b horizon (buried horizon) in Crosta and Dal Negro (2003). These results agree with the values obtained by De Vita et al. (2013), and Tufano et al. (2021b) for the B horizon. Moreover, for these soils, the contribution of cohesion to the shear strength was negligible due to the low amount of clayey fraction detected in the tested material (< 2%), unlike other researchers that considered a range of variation of cohesion values (Table 2) related to both root reinforcement and grain crushing (e.g., Tufano et al., 2021b). Good matches were also found for the unit weight value.

The results of propagation modeling provide information on the evolution of the 2019 Palma Campania landslide, simulating the deposit's thickness and the velocity distribution along the propagation path. Comparable to other precedential cases that occurred in the Campania region (e.g., Sarno landslides, Revellino et al., 2004; Nocera Inferiore landslide, Revellino et al., 2013), the modeled runout occurred with considerable velocity along an existing channel (Fig. 10). This condition played a controlling role in the development of the landslide phenomenon, which evolved from a debris slide to a debris flow. The transformation into a debris avalanche was prevented by the shape of the slope and the presence of the hydrographic network. Additionally, a check dam at the base of the slope significantly affected the safeguarding of the inhabited foothill. The modeling results reveals the deposit split. This mitigation measure is likely responsible for the short distance covered by the landslide. In the peri-Vesuvian slopes, the runout usually varies between several tens of meters and a few kilometers (Calcaterra et al., 2003). Accurately predicting such distance, as well as the magnitude of the depositional zones, landslide velocity, volume, and discharge, is essential for the design of mitigating measures. Notably, landslide propagation was simulated using the Voellmy (1955) rheological model in DAN-3D. This simplified approach considers the single-phase Voellmy rheology as representative of the flow behavior with

Table 2

Comparison between Mohr–Coulomb's shear strength parameters and unit weight values estimated in this study and literature data for the B horizon (De Vita et al., 2013; Tufano et al., 2021). Class "A" in Bilotta et al. (2005) and Cascini et al. (2005) denotes ashy soils with a fiwit grain size distribution, while class "B" denotes ashy soils with higher porosity values and lower specific gravity. In Crosta and Dal Negro (2003), B_b denotes the buried horizons, B_t denotes clay accumulation, and B_w denotes little or no clear illuvial accumulation of materials.

	Horizon	c' (kPa)	φ (°)	γ (kN/m³)
Laboratory tests	B	0.00	43	10.64
Tufano et al., 2021b	B	1.47–8.14	38–55	
De Vita et al., 2013	B	4.10–11.25	26–56	7.30–12.90
Bilotta et al., 2005	Class "A"	<2.94	30–35	6.58–9.50
	Class "B"	<2.94	36–41	5.71–12.32
Cascini et al., 2005	Class "A"	4.90–15.00	32–35	
	Class "B"	0.00–4.90	36–41	
Crosta and Dal Negro, 2003	B_b	34.02	39	7.20–9.90
	B_t	0.00–15.00	38–45	
	B_w	10.00–18.34	36–46	

respect to the calibrated parameters. In this particular case, no data regarding the propagation velocity was available, thus this parameter was not considered during the trial-and-error calibration. This had some implications on the results, such as uncertainty in the velocity distribution, the shape of the propagation zone and runout distance, and the thickness of the deposited material, some of which were partially different from those observed in the field. Similarly, in previous applications of the propagation model with DAN-3D in the volcanic context of Campania (e.g., Revellino et al., 2004, 2013), the propagation model includes uncertainties related to the rheology model and the calibrated parameters.

5.2. Slope evolution and implications for residual hazard

Results from the analyses indicated that the 2019 Palma Campania landslide (i) involved reworked pyroclastic deposits of an estimated average thickness of ~1.2 m, (ii) entrained a limited amount of slope sediment along the upper propagation zone, and (iii) entrained a limited amount of woody debris, mostly consisting of shrubs. The observed limited sediment entrainment suggests that the initial landslide volume of 450 m³ approximately corresponds to the final volume, making this landslide distinct from the more significant events that have occurred in the peri-Vesuvian area (Del Prete et al., 1998; Calcaterra and Santo, 2004; Revellino et al., 2004, 2013). This characteristic may indicate control of the local geologic setting (i.e., stratigraphy and slope sediment availability) in relation to the decadal geomorphological evolution of the slope. The presence of reworked deposits in the upper part of the slope may be linked to past landslides and/or erosion processes, which were unable to completely remove the slope-covering materials but were capable of reworking them. Such landslides would likely have been characterized by a magnitude lower than the 2019 landslide and a different mechanism (e.g., debris slide). Rapid-moving debris-slide debris-flow or debris-avalanches (Hungr et al., 2014) involving primary pyroclastic deposits tend to remove most slope sediment and deposit it at alluvial fans or the base of the slope (Revellino et al., 2004, 2013). Debris slides can cause the reworking and sediment redistribution of primary pyroclastic deposits along a slope, and their magnitude may be sufficiently low to prevent the complete removal of slope deposits (e.g., Guerriero et al., 2019). Sheet erosion over a long period may also contribute to this. The potential occurrence of such landslides or erosion processes may explain the limited amount of sediment available along the landslide path to be entrained. Although the 2019 landslide primarily propagated along a channel in which pyroclastic deposits can be expected to be absent due to erosion processes, the low amount of entrained sediment from the upper part of the slope, where the landslide propagates outside of the channel, can be attributed to its limited thickness. Additionally, the presence of shrub vegetation may corroborate the events that prevented the development of tree vegetation in the neighboring slope sectors.

Guadagno et al. (1988) indicated that primary deposits cropped out in the upper and middle parts of the western sector of the Crocelle slope, which was involved in the 1986 landslide. These deposits appear to be characterized by a thickness generally >5 m, except for the upper part of the slope, where lower thicknesses were observed. The 1986 landslide (i) involved layered pyroclastic deposits of an estimated average thickness of ~2 m, (ii) entrained a significant amount of slope sediment along the upper and middle parts of the slope, and (iii) entrained a significant volume of woody debris. A total volume estimated at 20,000 m³ was involved in the landslide. This noteworthy volume results from the consistent volumetric growth of the landslide along its path through sediment entrainment. Field observations conducted by Guadagno et al. (1988) indicated that this process occurred along the upper and middle parts of the slope, corresponding to the main transit zone of the landslides. The presence of primary deposits in the upper and middle sectors of the slope suggests the absence of significant past landslides and/or erosion processes, which could have caused the reworking or removal of

the deposits. The presence of a more substantial vegetation cover compared with the eastern sector of the slope may corroborate this interpretation.

Based on this evidence, two different conditions of landslide initiation and evolution along the Crocelle slope can be inferred. The first, represented by the 1986 landslide, depicts the occurrence of a significant magnitude landslide (i.e., volume) along a slope that was likely not previously affected by any past events. The second, represented by the 2019 landslide, reveals a limited-magnitude event along a slope that may have been previously affected by landslides. Each condition would represent a specific step in the decadal geomorphologic evolution of a pyroclastic-covered slope, indicating that a general decrease in landslide magnitude could be anticipated over time due to a reduction in slope sediment availability in relation to landslide and erosion processes. This interpretation may be reasonable in the absence of sediment supply in the form of volcanic eruptions or bedrock weathering. However, in the event of a new eruption (e.g., from the Somma-Vesuvio), fresh sediment would be supplied to neighboring slopes, creating the conditions for new significant magnitude landslides.

Significant implications of this statement are related to the evaluation of residual landslide hazards at recurrent landslide sites. Specifically, landslide hazard analysis can be simplified to determining landslide intensity and frequency (Fell et al., 2008; Fig. 12). With regard to fast-moving landslides affecting slopes covered by pyroclastic deposits (e.g., debris-slide debris-avalanche and/or debris-flow; Hungr et al., 2014), landslide intensity is contingent upon predisposing factors such as morphometric characteristics (slope angle and slope length), geological composition (stratigraphic setting and slope sediment) and vegetation, which may be completely or partially removed by landslides. Similarly, landslide frequency is related to rainfall regimes, which may be altered due to climate change (Gariano and Guzzetti, 2016), geological elements (stratigraphic setting and slope sediment) that can be transformed due to landslides or erosion processes, the presence of slope anomalies generated by human activity (i.e., slope trails), antecedent conditions of the slope that can modulate the effectiveness of

rainfall events in triggering a landslide event and vegetation, which can be totally or partially removed by landslides. The occurrence of landslides and erosion processes along a slope covered by pyroclastic deposits can lead to alterations in factors influencing both landslide intensity and frequency, resulting in a potential decrease in hazard. Indeed, although past landslides and erosion processes may attenuate prospective landslide magnitude by removing slope sediment, this action can also reduce the likelihood of new landslides (i.e., frequency). Analysis from De Vita et al. (2013) and Tufano et al. (2021a) have demonstrated that primary deposits are more prone to landslides due to their particular stratigraphic arrangement (i.e., interbedded pumice layer) and associated hydrologic behavior. Additionally, a continuous cover of pyroclastic deposits could heighten the overall susceptibility to slope landslides by increasing the surface area that could fail. Vegetation typically functions in two ways with respect to slope stability: i) increasing matric potential by decreasing water contents and enhancing cohesion by root tensile strength, and ii) by loading slope deposits. The implications of this potential hazard reduction are twofold: i) commonly-used approaches, based on magnitude-equivalent scenarios, may lead to an overestimation of residual landslide hazard and ii) mitigation measures for risk reduction should be designed with an event likely to occur in mind.
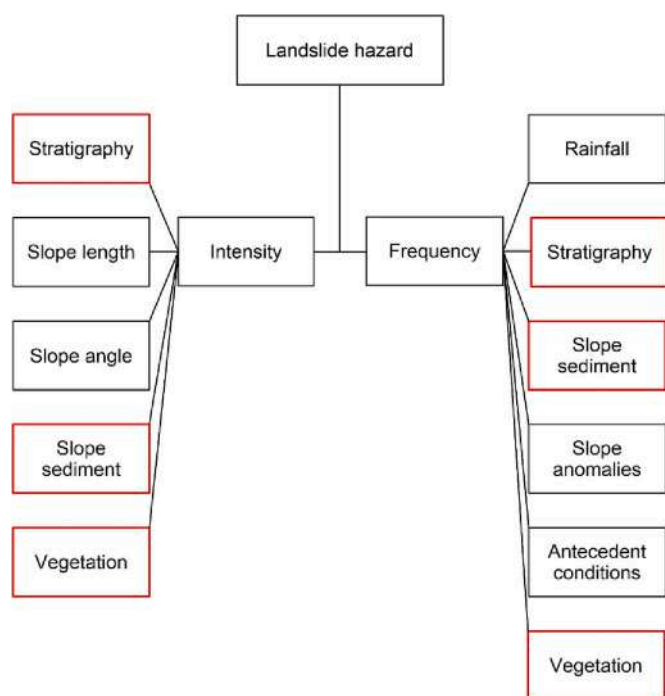
6. Conclusions

The 2019 Palma Campania landslide, identified as a debris-slide progressing to a debris flow, occurred along the Crocelle slope that had previously been affected by similar phenomena, as evidenced by the event that took place in February 1986. This event offered an opportunity to gain insight into the initiation and propagation conditions of the landslide and develop a better understanding of the evolution of residual landslide hazard at recurrent landslide sites. To this end, a combination of techniques were used, including UAV-aided field survey, geotechnical laboratory testing, statistical analysis of triggering rainfall, slope stability analysis, and propagation modeling. The results indicated that the landslide likely initiated after 13 h from the start of the rainfall event and that antecedent conditions played a significant role in slope failure. It was determined that a 4-year return period event was sufficient to initiate the landslide. The propagation modeling showed that the landslide mass reached the base of the slope after approximately 60 s, with the maximum velocity reaching 10 m/s. The deposits maintained a thickness of approximately 1 m during the propagation path and assumed a fan-shaped form at the base of the slope due to a check dam that divided the deposits into two fans.

Comparison with the 1986 event revealed a significant difference in the magnitude of the landslides (i.e., volume), which could be attributed to the different initial stratigraphic conditions and distributions of both slope sediment and vegetation. This discrepancy in terms of the decadal morphological evolution of slopes covered by pyroclastic deposits suggests that the occurrence of multiple landslides along a slope may reduce residual landslide hazard, resulting in a decrease in the expected magnitude and frequency of future events. This model can be used to explain the evolution of residual landslide hazard on many slopes covered by pyroclastic deposits that have been impacted by multiple landslides, and has implications for the potential overestimation of residual landslide hazards that results from the commonly-used magnitude-equivalent approach and the necessity for designing mitigation measures for risk reduction based on an event that is likely to occur. Implementing such measures would bring about considerable economic and environmental benefits.

Fig. 12. The flow chart showing landslide hazard factors. Red boxes indicate significant factors for landslide hazard modulation at recurrent landslide sites (i.e., residual hazard conditions). (For interpretation of the references to colour in this figure legend, the reader is referred to the web version of this article.)

CRediT authorship contribution statement

Methodology, Software, Formal analysis, Investigation, Data curation, Writing – original draft. **Francesco Fusco:** Conceptualization, Methodology, Software, Formal analysis, Investigation, Data curation, Writing – original draft, Visualization. **Rita Tufano:** Conceptualization, Methodology, Software, Formal analysis, Data curation, Writing – original draft, Visualization. **Enza Vitale:** Conceptualization, Methodology, Software, Formal analysis, Data curation, Writing – original draft, Visualization. **Luigi Guerriero:** Conceptualization, Methodology, Software, Formal analysis, Investigation, Data curation, Writing – original draft, Writing – review & editing, Visualization, Supervision.

Declaration of Competing Interest

The authors declare that they have no known competing financial interests or personal relationships that could have appeared to influence the work reported in this paper.

Data availability

Data will be made available on request.

Acknowledgements

References

Benz, W., 1990. Smooth particle hydrodynamics: A review. In: Buchler, J.R. (Ed.), The Numerical Modelling of Nonlinear Stellar Pulsatations. Kluwer Academic Publishers, Berlin, pp. 269–288. https://doi.org/10.1007/978-94-009-0519-1_16.

Bilotta, E., Cascini, L., Foresta, V., Sorbino, G., 2005. Geotechnical characterisation of pyroclastic soils involved in huge flowslides. Geotech. Geol. Eng. 23, 365–402. https://doi.org/10.1007/s10706-004-1607-3.

Caine, N., 1980. The rainfall intensity-duration control of shallow landslides and debris flows. Geografiska Annaler: Series A, Phys. Geogr. 62 (1–2), 23–27. https://doi.org/10.2307/520449.

Calcaterra, D., Santo, A., 2004. The January 10, 1997 Pozzano landslide, Sorrento Peninsula, Italy. Eng. Geol. 75 (2), 181–200.

Calcaterra, D., Parise, M., Palma, B., Pelella, L., 1999. The May 5th 1998 landsliding event in Campania, Southern Italy: Inventory of slope movements in the Quindici area. In Slope stability engineering, pp. 1361–1366.

Calcaterra, D., Parise, M., Palma, B., Pelella, L., 2000a. The influence of meteoric events in triggering shallow landslides in pyroclastic deposits of Campania, Italy. In: Landslides in Research, Theory and Practice: Proceedings of the 8th International Symposium on Landslides held in Cardiff on 26–30 June 2000. Thomas Telford Publishing, pp. 1–209.

Calcaterra, D., Parise, M., Palma, B., Pelella, L., 2000b. Multiple debris-flows in volcaniclastic materials mantling carbonate slopes. In: Debris-Flow Hazards Mitigation: Mechanics, Prediction and Assessment, pp. 99–107.

Calcaterra, D., de Riso, R., Evangelista, A., Nicotera, M.V., Santo, A., Scotto Di Santolo, A., 2003. Slope instabilities in the pyroclastic deposits of the Phlegraean district and the carbonate Apennine (Campania, Italy). In: International Workshop on Occurrence and Mechanisms of Flows in Natural Slopes and Earthfills Iw-Flows2003, Sorrento, May, 14-16, 2003.

Canli, E., Mergili, M., Thiebes, B., Glade, T., 2018. Probabilistic landslide ensemble prediction systems: Lessons to be learned from hydrology. Nat. Hazards Earth Syst. Sci. 18, 2183–2202. https://doi.org/10.5194/nhess-18-2183-2018.

Capra, L., Lugo-Hubp, J., Borselli, L., 2003. Mass movements in tropical volcanic terrains: the case of Teziutlán (México). Eng. Geol. 69 (3–4), 359–379. https://doi.org/10.1016/S0013-7952(03)00071-1.

Cascini, L., Cuomo, S., Sorbino, G., 2005. Flow-like mass movements in pyroclastic soils: remarks on the modelling of triggering mechanisms. Italian Geotech. J. 4, 11–31.

Cascini, L., Cuomo, S., Guida, D., 2008. Typical source areas of May 1998 flow-like mass movements in the Campania region, Southern Italy. Eng. Geol. 96 (3–4), 107–125. https://doi.org/10.1016/j.enggeo.2007.10.003.

Chang, W.J., Chou, S.H., Huang, H.P., Chao, C.Y., 2021. Development and verification of coupled hydro-mechanical analysis for rainfall-induced shallow landslides. Eng. Geol. 293, 106337 https://doi.org/10.1016/j.enggeo.2021.106337.

Chen, H., Lee, C.F., 2004. Geohazards of slope mass movement and its prevention in Hong Kong. Eng. Geol. 76 (1–2), 3–25. https://doi.org/10.1016/j.enggeo.2004.06.003.

Conrad, J.L., Morphew, M.D., Baum, R.L., Mirus, B.B., 2021. HydroMet: a new code for automated objective optimization of hydrometeorological thresholds for landslide initiation. Water 13 (13), 1752. https://doi.org/10.3390/w13131752.

Crosta, G.B., Dal Negro, P., 2003. Observations and modelling of soil slip-debris flow initiation processes in pyroclastic deposits: the Sarno 1998 event. Nat. Hazards Earth Syst. Sci. 3 (1/2), 53–69. https://doi.org/10.5194/nhess-3-53-2003.

Cuomo, S., Pastor, M., Cascini, L., Castorino, G.C., 2014. Interplay of rheology and entrainment in debris avalanches: a numerical study. Can. Geotech. J. 51 (11), 1318–1330. https://doi.org/10.1139/cgj-2013-0387.

Damiano, E., Greco, R., Guida, A., Olivares, L., Picarelli, L., 2017. Investigation on rainwater infiltration into layered shallow covers in pyroclastic soils and its effect on slope stability. Eng. Geol. 220, 208–218. https://doi.org/10.1016/j.enggeo.2017.02.006.

De Vita, P., Piscopo, V., 2002. Influences of hydrological and hydrogeological conditions on debris flows in peri-vesuvian hillslopes. Nat. Hazards Earth Syst. Sci. 2 (1/2), 27–35. https://doi.org/10.5194/nhess-2-27-2002.

De Vita, P., Napolitano, E., Godt, J.W., Baum, R.L., 2013. Deterministic estimation of hydrological thresholds for shallow landslide initiation and slope stability models: Case study from the Somma-Vesuvius area of southern Italy. Landslides 10, 713–728. https://doi.org/10.1007/s10346-012-0348-2.

De Vita, P., Fusco, F., Tufano, R., Cusano, D., 2018. Seasonal and event-based hydrological and slope stability modeling of pyroclastic fall deposits covering slopes in Campania (Southern Italy). Water 10 (9), 1140. https://doi.org/10.3390/w11091915.

Del Prete, M., Guadagno, F.M., Hawkins, A.B., 1998. Preliminary report on the landslides of 5 May 1998, Campania, southern Italy. Bull. Eng. Geol. Environ. 57 (2), 113–129. https://doi.org/10.1007/s100640050028.

Di Crescenzo, G., Santo, A., 2005. Debris slides–rapid earth flows in the carbonate massifs of the Campania region (Southern Italy): morphological and morphometric data for evaluating triggering susceptibility. Geomorphology 66 (1–4), 255-276.-129.

Di Martire, D., De Rosa, M., Pesce, V., Santangelo, M.A., Calcaterra, D., 2012. Landslide hazard and land management in high-density urban areas of Campania region, Italy. Nat. Hazards Earth Syst. Sci. 12, 905–926. https://doi.org/10.5194/nhess-12-905-2012.

Fell, R., Corominas, J., Bonnard, C., Cascini, L., Leroi, E., Savage, W.Z., 2008. Guidelines for landslide susceptibility, hazard and risk zoning for land-use planning. Eng. Geol. 102 (3–4), 99–111. https://doi.org/10.1016/j.enggeo.2008.03.022.

Fiorillo, F., Guerriero, L., Capobianco, L., Pagnozzi, M., Revellino, P., Russo, F., Guadagno, F.M., 2019. Inventory of Vietri-Maiori landslides induced by the storm of October 1954 (southern Italy). J. Maps 15 (2), 530–537. https://doi.org/10.1080/17445647.2019.1626777.

Fredlund, D.G., Morgenstern, N.R., Widger, R.A., 1978. The shear strength of unsaturated soils. Can. Geotech. J. 15, 313–321. https://doi.org/10.1139/t78-029.

Fusco, F., De Vita, P., 2015. Hydrological behavior of ash-fall pyroclastic soil mantled slopes of the Sarno Mountains (Campania - Southern Italy). Rend. Online Soc. Geol. Ital. 35, 148–151. https://doi.org/10.3301/ROL.2015.86.

Fusco, F., Allocca, V., De Vita, P., 2017. Hydro-geomorphological modelling of ash-fall pyroclastic soils for debris flow initiation and groundwater recharge in Campania (southern Italy). Catena 158, 235–249. https://doi.org/10.1016/j.catena.2017.07.010.

Fusco, F., De Vita, P., Mirus, B.B., Baum, R.L., Allocca, V., Tufano, R., Di Clemente, E., Calcaterra, D., 2019. Physically based estimation of rainfall thresholds triggering shallow landslides in volcanic slopes of Southern Italy. Water 11, 1915. https://doi.org/10.3390/w11091915.

Fusco, F., Mirus, B.B., Baum, R.L., Calcaterra, D., De Vita, P., 2021. Incorporating the effects of complex soil layering and thickness local variability into distributed landslide susceptibility assessments. Water 13 (5), 713. https://doi.org/10.3390/w13050713.

Gariano, S.L., Guzzetti, F., 2016. Landslides in a changing climate. Earth Sci. Rev. 162, 227–252. https://doi.org/10.1016/j.earscirev.2016.08.011.

Godt, J.W., McKenna, J.P., 2008. Numerical modeling of rainfall thresholds for shallow landsliding in the Seattle, Washington, area. Rev. Eng. Geol. 20, 121–136. https://doi.org/10.1130/2008.4020(07).

Greco, R., Comegna, L., Damiano, E., Guida, A., Olivares, L., Picarelli, L., 2013. Hydrological modelling of a slope covered with shallow pyroclastic deposits from field monitoring data. Hydrol. Earth Syst. Sci. 17 (10), 4001–4013. https://doi.org/10.5194/hess-17-4001-2013.

Greco, R., Comegna, L., Damiano, E., Marino, P., Olivares, L., Santonastaso, G.F., 2021. Recurrent rainfall-induced landslides on the slopes with pyroclastic cover of Partenio Mountains (Campania, Italy): Comparison of 1999 and 2019 events. Eng. Geol. 288, 106160.

Guadagno, F., 1991. Debris flows in the Campanian volcaniclastic soils. In: Proc., Slope Stability Engineering: Developments and applications: Proceedings of the International Conference on Slope Stability. https://doi.org/10.1680/ssedaa.16606.0021.

Guadagno, F.M., Palmieri, M., Siviero, V., Vallario, A., 1988. La frana di Palma Campania. Geol. Tec. 4, 18–29 (In Italian).

Guadagno, F.M., Forte, R., Revellino, P., Fiorillo, F., Focareta, M., 2005. Some aspects of the initiation of debris avalanches in the Campania Region: the role of morphological

slope discontinuities and the development of failure. Geomorphology 66 (1–4), 237–254. https://doi.org/10.1016/j.geomorph.2004.09.024.

Guerriero, L., Guadagno, F.M., Revellino, P., 2019. Estimation of earth-slide displacement from GPS-based surface-structure geometry reconstruction: estimation of earth-slide displacement. Landslides 16, 425–430. https://doi.org/10.1007/s10346-018-1091-0.

Harp, E.L., Reid, M.E., McKenna, J.P., Michael, J.A., 2009. Mapping of hazard from rainfall-triggered landslides in developing countries: examples from Honduras and Micronesia. Eng. Geol. 104 (3–4), 295–311. https://doi.org/10.1016/j.enggeo.2008.11.010.

Hsieh, P.A., Wingle, W., Healy, R.W., 2000. VS2D—a graphical software package for simulating fluid flow and solute or energy transport in variably saturated porous media. In: U.S. Geological Survey. Water-Resources Investigations Report 9–4130.

Hungr, O., 1995. A model for the runout analysis of rapid flow slides, debris flows, and avalanches. Can. Geotech. J. 32 (4), 610–623. https://doi.org/10.1139/t95-063.

Hungr, O., Evans, S.G., 2004. Entrainment of debris in rock avalanches: an analysis of a long run-out mechanism. Geol. Soc. Am. Bull. 116 (9–10), 1240–1252. https://doi.org/10.1130/B25362.1.

Hungr, O., Leroueil, S., Picarelli, L., 2014. The Varnes classification of landslide types, an update. Landslides 11, 167–194. https://doi.org/10.1007/s10346-013-0436-y.

Iverson, R.M., 2000. Landslide triggering by rain infiltration. Water Resour. Res. 36 (7), 1897–1910. https://doi.org/10.1029/2000WR900090.

Iverson, R.M., 2012. Elementary theory of bed-sediment entrainment by debris flows and avalanches. J. Geophys. Res. Earth Surf. 117 (F3).

Jenkinson, A.F., 1955. The frequency distribution of the annual maximum (or minimum) values of meteorological elements. Quart. J. Royal Meteorol. Soc. 87, 145–158.

Lu, N., Likos, W.J., 2004. Unsaturated Soil Mechanics. Wiley, New York, p. 556.

Marin, R.J., García, E.F., Aristizábal, E., 2020. Effect of basin morphometric parameters on physically-based rainfall thresholds for shallow landslides. Eng. Geol. 278, 105855 https://doi.org/10.1016/j.enggeo.2020.105855.

McDougall, S., Hungr, O., 2004. A model for the analysis of rapid landslide motion across three-dimensional terrain. Can. Geotech. J. 41 (6), 1084–1097. https://doi.org/10.1139/t04-052.

Monaghan, J.J., 1992. Smoothed particle hydrodynamics. Annu. Rev. Astron. Astrophys. 30 (1), 543–574. https://doi.org/10.1146/annurev.aa.30.090192.002551.

Montgomery, D.R., Dietrich, W.E., 1994. A physically based model for the topographic control on shallow landsliding. Water Resour. Res. 30 (4), 1153–1171. https://doi.org/10.1029/93WR02979.

Muntohar, A.S., Ikhsan, J., Liao, H.J., Jotisankasa, A., Jetten, V.G., 2022. Rainfall Infiltration-induced Slope Instability of the Unsaturated Volcanic Residual Soils during Wet Seasons in Indonesia. Indonesian J. Geosci. 9 (1), 71–85.

Napolitano, E., De Vita, P., Fusco, F., Allocca, V., Manna, F., 2015. Long-term hydrological modelling of pyroclastic soil mantled slopes for assessing rainfall thresholds triggering debris flows: The case of the Sarno Mountains (Campania—southern Italy). In: Engineering Geology for Society and Territory-Volume 2: Landslide Processes. Springer International Publishing, pp. 1567–1570. https://doi.org/10.1007/978-3-319-09057-3_278.

Napolitano, E., Fusco, F., Baum, R.L., Godt, J.W., De Vita, P., 2016. Effect of antecedent hydrological conditions on rainfall triggering of debris flows in ash-fall pyroclastic mantled slopes of Campania (southern Italy). Landslides 13 (967–983), 4. https://doi.org/10.1007/s10346-015-0647-5.

Patacca, E., Scandone, P., 2007. Geology of the Southern Apennines. In: Mazzotti, A., Patacca, E., Scandone P. (Eds.), CROP-04, Special Issue, Italian Journal of Geosciences, vol. 7, pp. 75–119.

Pradhan, S., Toll, D.G., Rosser, N.J., Brain, M.J., 2022. An investigation of the combined effect of rainfall and road cut on landsliding. Eng. Geol. 307, 106787 https://doi.org/10.1016/j.enggeo.2022.106787.

Rahardjo, H., Kim, Y., Satyanaga, A., 2019. Role of unsaturated soil mechanics in geotechnical engineering. Int. J. Geo-Eng. 10, 1–23. https://doi.org/10.1186/s40703-019-0104-8.

Revellino, P., Hungr, O., Guadagno, F.M., Evans, S.G., 2004. Velocity and runout simulation of destructive debris flows and debris avalanches in pyroclastic deposits, Campania region, Italy. Environ. Geol. 45 (3), 295–311. https://doi.org/10.1007/s00254-003-0885-z.

Revellino, P., Guerriero, L., Grelle, G., Hungr, O., Fiorillo, F., Esposito, L., Guadagno, F. M., 2013. Initiation and propagation of the 2005 debris avalanche at Nocera Inferiore (Southern Italy). Ital. J. Geosci. 132 (3), 366–379. https://doi.org/10.3301/IJG.2013.02.

Rianna, G., Pagano, L., Urciuoli, G., 2014. Rainfall patterns triggering shallow flowslides in pyroclastic soils. Eng. Geol. 174, 22–35.

Santacroce, R., Cioni, R., Marianelli, P., Sbrana, A., Sulpizio, R., Zanchetta, G., Donahue, D.J., Joron, J.L., 2008. Age and whole rock–glass compositions of proximal pyroclastics from the major explosive eruptions of Somma-Vesuvius: a review as a tool for distal tephrostratigraphy. Journal of Volcanology and Geothermal Research, 177, 1–18. Sci. 12, 905–926. https://doi.org/10.1016/j.jvolgeores.2008.06.009.

Santo, A., Di Crescenzo, G., Forte, G., Papa, R., Pirone, M., Urciuoli, G., 2018. Flow-type landslides in pyroclastic soils on flysch bedrock in southern Italy: the Bosco de'Preti case study. Landslides 15 (1), 63–82. https://doi.org/10.1007/s10346-017-0854-3.

Sepe, C., Calcaterra, D., Cecconi, M., Di Martire, D., Pappalardo, L., Scarfone, R., Vitale, E., Russo, G., 2021a. Formation of capillary barriers during rainfall events in pyroclastic deposits in the Vesuvian area. Geosciences 2021, 11. https://doi.org/10.3390/geosciences11070274.

Sepe, C., Calcaterra, D., Di Martire, D., Ramondini, M., Russo, G., Vitale, E., Pappalardo, L., 2021b. Landslide susceptibility assessment in pyroclastic soils: numerical analysis on the role of capillary barriers. In: IJEGE.2021-01.S-20. https://doi.org/10.4408/IJEGE.2021-01.S-20.

Smith, D.M., Oommen, T., Bowman, L.J., Gierke, J.S., Vitton, S.J., 2015. Hazard assessment of rainfall-induced landslides: a case study of San Vicente volcano in Central El Salvador. Nat. Hazards 75 (3), 2291–2310. https://doi.org/10.1007/s11069-014-1422-y.

Sun, P., Wang, H., Wang, G., Li, R., Zhang, Z., Huo, X., 2021. Field model experiments and numerical analysis of rainfall-induced shallow loess landslides. Eng. Geol. 295, 106411 https://doi.org/10.1016/j.enggeo.2021.106411.

Tufano, R., Fusco, F., De Vita, P., 2016. Spatial modeling of ash-fall pyroclastic deposits for the assessment of rainfall thresholds triggering debris flows in the Sarno and Lattari mountains (Campania, southern Italy). Rend. Online Soc. Geol. Ital. 41, 210–213. https://doi.org/10.3301/ROL.2016.131.

Tufano, R., Cesarano, M., Fusco, F., De Vita, P., 2019. Probabilistic approaches for assessing rainfall thresholds triggering shallow landslides. The study case of the peri-Vesuvian area (southern Italy). Italian J. Eng. Geol. Environ. Special 1. https://doi.org/10.4408/IJEGE.2019-01.S-17.

Tufano, R., Formetta, G., Calcaterra, D., De Vita, P., 2021a. Hydrological control of soil thickness spatial variability on the initiation of rainfall-induced shallow landslides using a three-dimensional model. Landslides 18, 3367–3380. https://doi.org/10.1007/s10346-021-01681-x.

Tufano, R., Annunziata, L., Di Clemente, E., Falgiano, G., Fusco, F., De Vita, P., 2021b. Analysis of shear strength variability of ash-fall pyroclastic soils involved in flow-like landslides. In: Tiwari, B., Sassa, K., Bobrowsky, P.T., Takara, K. (Eds.), Understanding and Reducing Landslide Disaster Risk. WLF 2020. ICL Contribution to Landslide Disaster Risk Reduction. Springer, Cham. https://doi.org/10.1007/978-3-030-60706-7_32.

Urciuoli, G., Pirone, M., Comegna, L., Picarelli, L., 2016. Long-term investigations on the pore pressure regime in saturated and unsaturated sloping soils. Eng. Geol. 212, 98–119.

van Genuchten, M.T., 1980. A closed form equation for predicting the hydraulic conductivity of unsaturated soils. Soil Sci. Soc. Am. J. 44, 892–898. https://doi.org/10.2136/sssaj1980.03615995004400050002x.

Vitale, S., Ciarcia, S., 2018. Tectono-stratigraphic setting of the Campania region (southern Italy). J. Maps 14 (2), 9–21. https://doi.org/10.1080/17445647.2018.142.

Voellmy, A., 1955. Uber die Zerstorungskraft von Lawinen. Schweizerische Bauzeitung, Jahrg. 73, 159–162 (In German).

Wu, L.Z., Zhou, Y., Sun, P., Shi, J.S., Liu, G.G., Bai, L.Y., 2017. Laboratory characterization of rainfall-induced loess slope failure. Catena 150, 1–8. https://doi.org/10.1016/j.catena.2016.11.002.

Yang, H.Q., Zhang, L., Gao, L., Phoon, K.K., Wei, X., 2022. On the importance of landslide management: Insights from a 32-year database of landslide consequences and rainfall in Hong Kong. Eng. Geol. 299, 106578.

Zhu, S.R., Wu, L.Z., Song, X.L., 2022. An improved matrix split-iteration method for analyzing underground water flow. Eng. Comput. 1-17 https://doi.org/10.1007/s00366-021-01551-z.